JACS
JOURNAL OF THE AMERICAN CHEMICAL SOCIETY
pubs.acs.org/JACS
Article

Electron–Phonon Coupling in Current-Driven Single-Molecule Junctions

Hai Bi,[○] Carlos-Andres Palma,*[,○] Yuxiang Gong, Klara Stallhofer, Matthias Nuber, Chao Jing, Felix Meggendorfer, Shizheng Wen, ChiYung Yam, Reinhard Kienberger, Mark Elbing, Marcel Mayor, Hristo Iglev,* Johannes V. Barth,* and Joachim Reichert*

Cite This: J. Am. Chem. Soc. 2020, 142, 3384–3391

Read Online

ACCESS | Metrics & More | Article Recommendations | Supporting Information

ABSTRACT: Vibrational excitations provoked by coupling effects during charge transport through single molecules are intrinsic energy dissipation phenomena, in close analogy to electron–phonon coupling in solids. One fundamental challenge in molecular electronics is the quantitative determination of charge-vibrational (electron–phonon) coupling for single-molecule junctions. The ability to record electron–phonon coupling phenomena at the single-molecule level is a key prerequisite to fully rationalize and optimize charge-transport efficiencies for specific molecular configurations and currents. Here we exemplarily determine the pertaining coupling characteristics for a current-carrying chemically well-defined molecule by synchronous vibrational and current–voltage spectroscopy. These metal-molecule-metal junction insights are complemented by time-resolved infrared spectroscopy to assess the intramolecular vibrational relaxation dynamics. By measuring and analyzing the steady-state vibrational distribution during transient charge transport in a bis-phenylethynyl-anthracene derivative using anti-Stokes Raman scattering, we find ∼0.5 vibrational excitations per elementary charge passing through the metal-molecule-metal junction, by means of a rate model ansatz and quantum-chemical calculations.

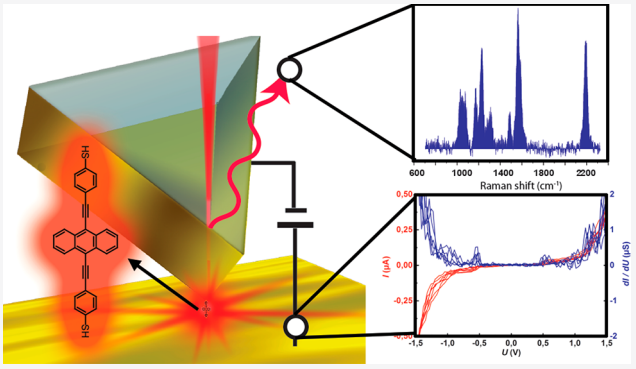

INTRODUCTION

Understanding and controlling loss mechanisms during charge transport through single molecules is fundamental for the development of molecule-based nanoelectronic device elements.[1−3] During conduction through individual molecular species, charge from an electrode can transfer through the energy levels of a (vibrationally excited) molecule and subsequently populate states of a second lead. In metal-molecule-metal junctions,[4−11] where individual π-conjugated molecules may show conductances near 0.5 μS,[4,8−10] electrode–molecule and electron–phonon coupling[12,13] (or, more specifically for molecules, charge-vibrational coupling) play an important role in the resistivity characteristics.[10,14−18] Thus, the understanding and control over electron–phonon coupling (EPC), which can be represented by a dimensionless constant λ,[14,19,20] would enable the optimization of a wide range of conductance properties,[1] including, for example, enhancement or suppression[21,22] of dissipation channels. Calculation schemes have been employed to determine the EPC, yielding values from 0.34 to 0.02 for coupling to low-energy modes in benzene.[14,19]

Yet, the experimental determination of EPC in single molecules remains a challenging issue. This is especially demanding for systems with strong vibrational coupling, often encountered in double-barrier molecular[23−25] or Coulomb blockade junctions.[21,26−29] In the strong vibrational coupling regime, markedly different from coherent transport,[30] charging of the molecule and subsequent relaxation to the neutral state can interfere,[24,31−33] bringing the molecule toward a higher-level vibrational state. Moreover, experimental evidence for bias-induced shifts of vibrational frequencies, indicative of coupling between electronic excitation and molecular vibrations, have been associated with (transient) charging effects[34,35] or symmetry changes.[36,37]

One proposed strategy toward measuring the EPC in realistic configurations with energy dissipation is to record the steady-state vibrational population during transport.[32,38,39] By using a molecular junction spectroscopy (MJS) setup, the concurrent monitoring of both the vibrational population by calibrated Raman spectroscopy and the current in a single-molecule junction becomes possible. Here, we use this method for a 9,10-bis-phenylethynyl-anthracene molecule connected to

Received: July 20, 2019
Published: February 4, 2020

https://dx.doi.org/10.1021/jacs.9b07757
J. Am. Chem. Soc. 2020, 142, 3384–3391

electrodes with terminal thiol anchor groups (**BPA**, see Figure 1a). While applying and sweeping a bias voltage, we find a gap region followed by an abrupt change to a charge transport region above a certain voltage threshold. The concomitantly recorded Stokes Raman signal unambiguously reveals that transport occurs through the highest occupied molecular orbital (HOMO) and that the molecule should be regarded as transiently charged, as indicated by density functional theory (DFT) simulations. In the identified transport regime, we detect an anti-Stokes Raman signal. This spectrum, combined with current characteristics of the junction and the measurement of intramolecular vibrational relaxation times, grants access to an EPC constant λ by means of a simple rate equation model combined with quantum-chemical computations.

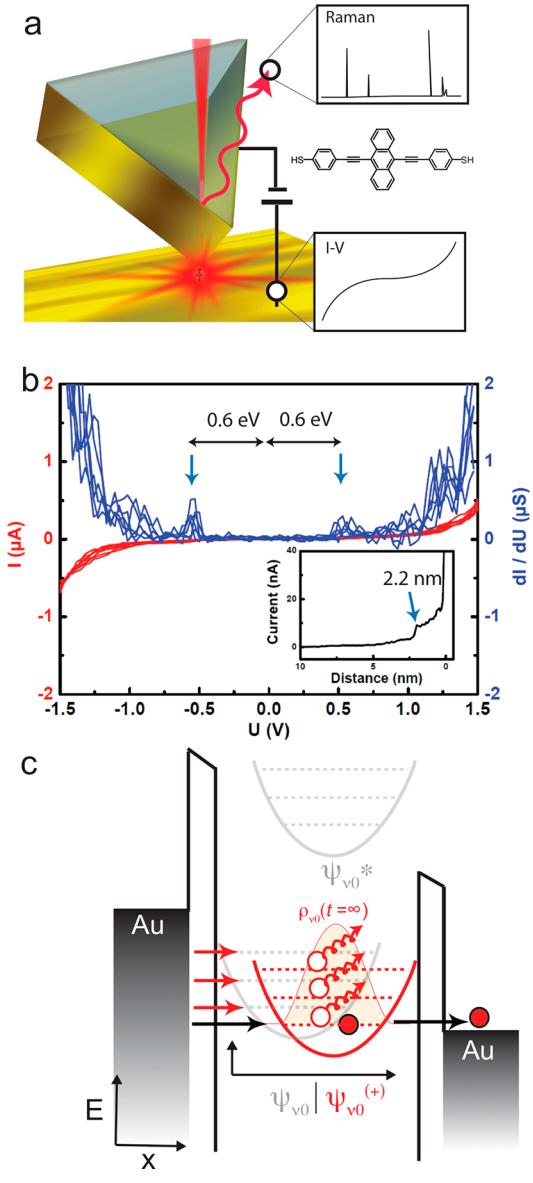

Figure 1. Contacting and characterizing a single molecule. (a) MJS setup illustrating a single **BPA** molecular junction with gold contacts. (b) Typical processed current-voltage (I–U, red) characteristics and current derivatives (dI/dU, blue) selected from a raw set of 2491 curves (see Supporting Information Figure S1 for complete data set). (inset) A representative current-distance (I–Z) approach curve at U = 0.5 V employed as an indicator of molecular junction formation, whereby contact is established approximately at 2.2 nm (I = 10 ± 1 nA) from the short-circuit region. (c) Schematics of charge transport through the HOMO. The adiabatic curve (red shaded area) illustrates EPC proportional to the coordinate displacement[1] between the wave functions $\psi^{(+)}$ and ψ, associated with a charged and neutral state, respectively. Possible elastic channels (black arrows), inelastic channels (red arrows), and the evolving steady-state vibrational distribution (ρ) are illustrated.

EXPERIMENTAL SECTION

Molecular Junction Spectroscopy. The MJS setup presents a new method for studying charge transport through single molecules in strong optical fields. The rodlike, thiol-terminated **BPA** molecules are covalently anchored to a gold film through self-assembly techniques and contacted from the other side by the apex of a gold-covered (20 nm) tetrahedral glass (T-tip) fragment.[40,41] The tip–sample distance is controlled by a piezo crystal. The technique integrates a home-built Raman spectroscopy setup (Supporting Information Figure S2). The laser light (He–Ne laser, 12 mW, 632.8 nm) is coupled through the backside of the glass body of the tetrahedral glass fragment into the apex of the tip. The tip acts as the light source, counter-electrode, and light collector at the same time (Figure 1a). All measurements shown are recorded at room temperature in high vacuum (~$1\cdot10^{-7}$ mbar) to prevent the molecules from decomposing in the presence of oxygen.[42] By heating the whole setup during control measurements, we estimated that the temperature remained clearly below 100 °C in the junction, at which temperature the molecules decompose without showing similar effects in the anti-Stokes Raman spectra (Supporting Information Figure S3).

Substrate Preparation. The fabrication process of the glass substrate is the same as for the T-tip. The glass slide is coated with a 200–500 nm gold film, whose roughness is ~20–30 nm. A droplet of **BPA** dissolved in tetrahydrofuran (0.5 mM) is deposited with a pipet on the gold-covered substrate. Then the solution covered substrate is put in an atmosphere saturated with tetrahydrofuran for 3 h, to allow the molecules to anchor covalently to the substrate.

Molecular Junction Preparation. After preparing the sample ex situ and fixing it on the sample holder in the vacuum chamber, the tip is approached mechanically into the working distance of the piezo crystal with the help of a tunneling current feedback loop. For all subsequent measurements the tip–sample distance was controlled manually by the piezo voltage. The setup deliberately lacks the ability to move or image the substrate laterally to minimize internal and external disturbances and to ensure the highest possible stability of the formed junctions. Figure 1b inset depicts a typical I–Z curve during successful formation of a single-molecule junction. At distances of ~2.2 nm, a (10 ± 1) nA current step at ~0.6 V (~0.02 μS) characteristic of the formation of a covalently linked metal-molecule-metal contact is distinguished and reproduced with high fidelity (the molecule has a sulfur–sulfur length of 2.0 nm). Following this, I–U curves are measured, and a conductance histogram is prepared (Supporting Information Figure S1). Raman spectra are recorded from junctions at the peak of the histogram, usually displaying from 1 to 300 μG_0 (G_0 = 7.74 × 10^{-5} S) at ~0.6 V. This method is commonly employed to narrow outlier metal-molecule-metal configurations.[43,44]

Femtosecond UV-IR Spectroscopy. The setup for pump–probe measurements is based on a commercial Ti:sapphire laser system (130 fs, 800 nm, 1 kHz, see Supporting Information for more details). Part of the output was frequency doubled to obtain pump pulses at 400 nm with an energy of 0.5 μJ. A two-stage optical parametric amplifier with subsequent difference frequency generation yield mid-IR probe pulses at 1500 cm^{-1} (spectral width ~200 cm^{-1}). The probe beams are spectrally resolved in a polychromator and recorded on a 2 × 64 pixel HgCdTe detector. The spectral resolution of the system is 2 cm^{-1}. The vibrational relaxation dynamics are monitored as the change in the optical density $\Delta OD = -\log(T/T_0)$, with T being the probe beam's transmission through an excited sample, and T_0 being the transmission through an unexcited sample, that is, with pump

https://dx.doi.org/10.1021/jacs.9b07757
J. Am. Chem. Soc. 2020, 142, 3384–3391

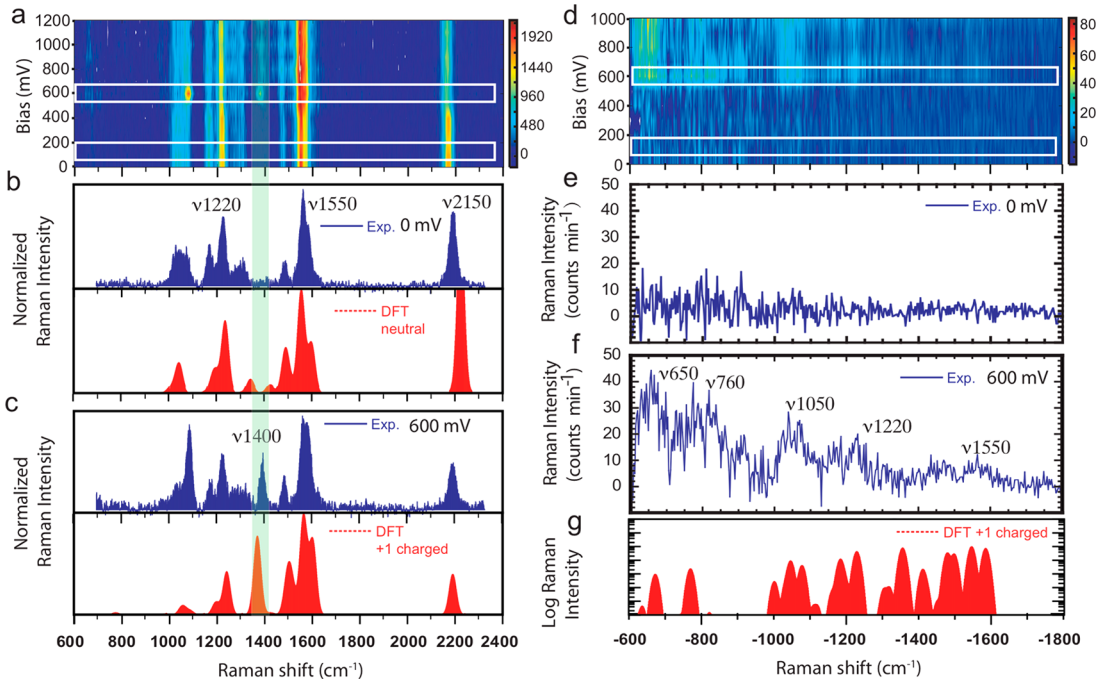

Figure 2. Single-molecule Raman spectroscopy. (a) Voltage-dependent Raman Stokes scattering from molecular junctions (see Supporting Information Figure S1 for additional data sets). The white rectangles in (a) highlight two spectral regions at and below the transport resonance at 0.6 V. (b) Measured (blue) and calculated (red) spectra of the neutral molecule. (c) Measured (blue) and calculated (red) spectra of the charged state. A characteristic mode at ∼1400 cm^{-1} (green bar) appears only for the simulated spectrum of the positively charged state (see text and Supporting Information Figure S5 for comparative theoretical studies and Supporting Information Figure S6 for negative bias data). (d) Voltage-dependent Raman anti-Stokes scattering. The white rectangles in (d) highlight two spectral regions above and below the resonance at 0.6 V. (e, f) Anti-Stokes spectra (e) below 0.6 V and (f) at 0.6 V. (g) The calculated spectrum in (c) is plotted in semilogarithmic scale for ease of comparison to the anti-Stokes spectrum. The excitation wavelength is 632.8 nm.

beam blocked. The probe beam polarization is adjusted to a magic angle setting (54.7°) with respect to the pump beam to avoid a possible induced optical anisotropy. The sample compartment is flushed with dry air to avoid absorption lines due to atmospheric water. The **BPA** dissolved in dichloromethane was pumped through a 90 μm thick CaF_2 flow cell from a reservoir in a closed cycle. To avoid degradation of the sample in the course of a longer measurement a large sample volume of 40 mL was used.

Density Functional Theory. Simulated Raman spectra were calculated with the quantum chemical package Firefly. Hartree and Hessian activities were obtained at the Perdew-Burke-Ernzerhof (PBE) level of theory (PBE86 in Firefly) using a 6-311G basis set. The stationary-state PBE geometry and Hessian of the neutral molecule were used as an input for calculating the Raman spectrum, employing the SOGGEX level of theory and a TZV 3p 3d basis set with diffuse *s* functions. Firefly calculations were performed by increasing the isotopic mass of the S and H elements of the thiol terminal groups to 1 000 000 amu, to simulate the immobilization of the thiols on the gold electrodes.

RESULTS AND DISCUSSION

After a junction has formed, *I*−*U* characteristics are recorded, which often reveal prominent features at ±0.6 V (Figure 1b shows a selected set of curves). An automatically processed current histogram of 2491 *I*−*U* curves is shown in Supporting Information Figure S1a. In conjunction with Raman evidence (see below), these channels are associated with charge transport through one of the molecular orbitals, which process is known to be accompanied by inelastic energy dissipation in the form of vibrational excitations[45] (Figure 1c). Accordingly, we explored the characteristics of these excitations by vibrational spectroscopy in the bias voltage range from 0 to ±1.2 V (Figure 2a). Raman spectroscopy measurements reveal no change in the Stokes spectra intensities in the [−0.6, +0.6] V bias interval (Figure 2b). At ∼0.6 V, new sharp signals appear close to 1080 and 1400 cm^{-1} in the Raman Stokes spectrum, whereas the peak at 2150 cm^{-1} is significantly reduced (Figure 2c). At voltages exceeding the resonance at 0.6 eV the peak at 1080 cm^{-1} vanishes. The spectral features appearing at 0.6 V strongly indicate that the acquired Raman signal originates exclusively from an individual, current-carrying molecule, because an average Raman spectrum from multiple bystanding molecules cannot be expected to produce sharp, articulated current-induced Raman signatures.

The new signals are rationalized with the help of simulated Raman spectra. In particular, different molecular charge states are investigated by DFT, employing constrained -SH moieties. The calculated vibrational characteristics of the neutral species matches the experimental spectrum up to ±0.6 V, whereas the spectral signature for higher bias can only be reproduced by invoking the simulation of a positive charged molecular state (with a correlation factor of $R = 0.27$ and offset scaling of just 3 cm^{-1}; see Supporting Information Figure S5 for the complete set of simulations). Notably, the ∼1400 cm^{-1} signal is absent from the DFT-calculated Raman spectrum of the neutral molecule (Figure 2b in red) and appears exclusively for the charged state in Figure 2c. Moreover, the respective calculated intensity from a single molecule coincides with the observed signal, as expected for the response of an individual species. These observations altogether substantiate the single-molecule emitter concept and strongly indicate that **BPA** undergoes transient charging during transport.

https://dx.doi.org/10.1021/jacs.9b07757
J. Am. Chem. Soc. 2020, 142, 3384−3391

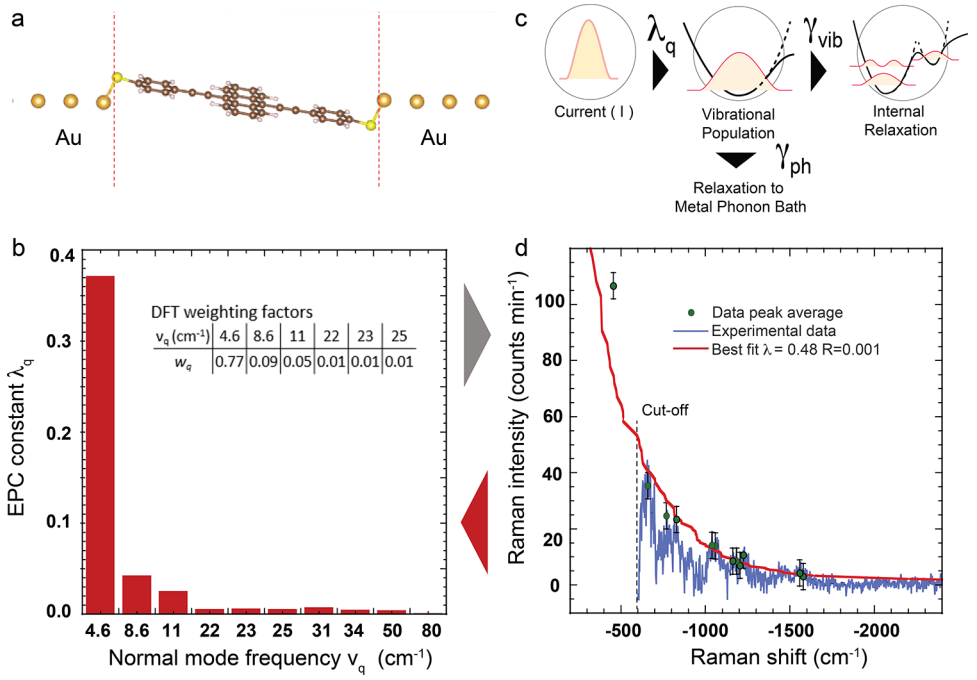

Figure 3. Electron−Phonon coupling rate model combined with quantum-chemical calculations. (a) DFT-optimized molecular geometry with fixed gold electrodes. (b) The weight w_q extracted from theory and the EPC constants λ_q obtained from the rate model in eq 2 (red). (c) A three-step rate model, where the coupling constant λ_q to the normal-mode frequency ν_q is calculated to be in steady-state equilibrium, with intramolecular relaxation through vibrational-vibrational rate γ_{vib} and with dissipation to the metal electrodes through a vibrational-phonon rate γ_{ph}. (d) The best fit (R-factor = 0.001) to the calibrated anti-Stokes Raman spectrum envelope (the peaks in Figure 2f) compared to the model envelope. The fit considers coupling to the calculated modes, starting at 4.6 cm^{-1}. Employing the measured internal relaxation time scale of $\tau_{vib} = \gamma_{vib}^{-1} = (37 \pm 4)$ ps, we find a total $\lambda = 0.48$ (see text). The additional anti-Stokes Raman mode 431 cm^{-1} became accessible by measuring with a 50% mirror instead of a broad bandwidth dichroic beam splitter (see Supporting Information Figure S4).

Remarkably, for voltages exceeding the ±0.6 V threshold of the transport resonance, an anti-Stokes Raman spectrum with a series of peaks appears. Three important implications follow from the occurrence of these signals. First, a sharp step in the intensity at ±0.6 V, together with the absence of continuous or quadratic shifts, exclude bias-mediated Stark effects.[34,35] Second, the fact that this distribution does not change with applied bias (Figure 2d) implies that the vibrational steady-state distribution cannot be attributed to resistive heating ($\sim V^2 \cdot R^{-1}$).[46−48] Third, the anti-Stokes spectrum follows a nonlinear decreasing envelope of the Raman active modes (Figure 2f,g; the calculated spectrum is shown in red). The latter is a strong indication that the distribution is not considerably affected by an electronic temperature background.[49] The exponential shape of the envelope is further supported by the measurement of an intense mode at 431 cm^{-1} (Supporting Information Figure S4).

Temperature-controlled experiments corroborate that the anti-Stokes spectra are not generated by nanoscopic laser or junction temperature effects. When heating the setup to ∼100 °C, stepwise molecular decomposition was identified by Raman spectroscopy (cf. Supporting Information Figure S3). At this temperature, only Stokes (no anti-Stokes) signals were observed at biases below 600 mV. At temperatures that already decompose the molecule, a significant population of vibrational modes should be expected. Obviously, our setup is not sensitive to such populations at the single-molecule level. This allows us to exclude that the anti-Stokes signal is originating from temperature effects, in marked contrast to multimolecular junctions subject to microwatt current power densities, a regime that has been thoroughly documented.[47,48,50] Field effects and current heating in molecular junctions have been reported previously, but they are dominant only in polarizable junctions and in junctions with a high conductance (>mG_0), respectively. Thus, we attribute our observations to EPC and vibrational-vibrational dissipation.[32,38,39] It follows that the detection of a steady-state, bias-independent, vibrational population during transient molecular charging enables the determination of a single-molecule EPC.

In a classical rate model,[32,38,39] vibrational modes ν_q, having a vibrational population of p_q, couple to the current I via coupling constants λ_q.[51] The rate of vibrational excitations is proportional to the current I and can be determined by the following formula:

$$\frac{dp_q}{dt} = \frac{I}{e} \cdot \lambda_q \tag{1}$$

Here e denotes the elementary charge. It is useful to define a total coupling constant as $\lambda = \sum_q \lambda_q$.[52] A calibrated anti-Stokes Raman spectrum provides direct access to vibrational populations via the number of absolute scattered phonons per second (dp_q/dt), while the current can be obtained from the molecular junction experiment. In our setup, the total number of collected anti-Stokes photons, which is a measurement of the total phonon population, is obtained by dividing the integrated anti-Stokes signal by the photon flux at the tip apex and accounting for the collection efficiency (see near-field Raman methods in the Supporting Information).

Rate models have been successfully employed[32] to accurately quantify an EPC constant from a steady-state distribution, provided that the intramolecular vibrational-

https://dx.doi.org/10.1021/jacs.9b07757
J. Am. Chem. Soc. 2020, 142, 3384−3391

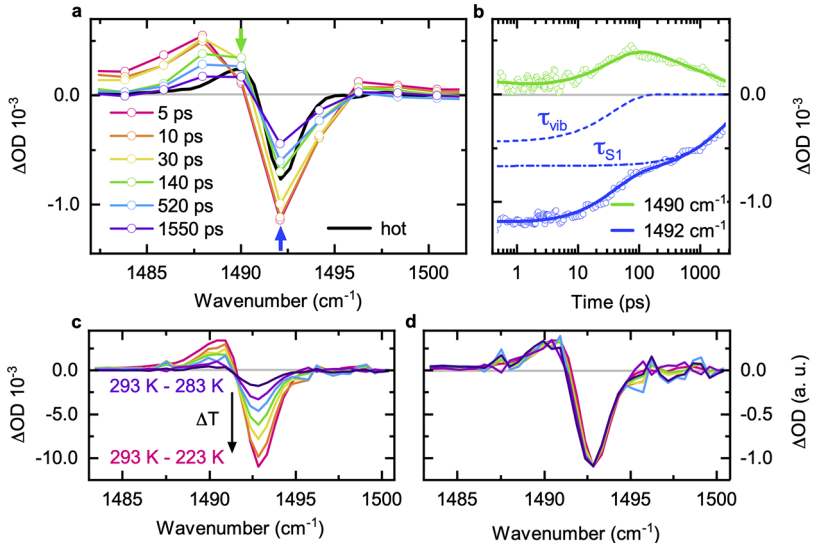

Figure 4. Vibrational relaxation of **BPA** in dichloromethane. (a) Time-resolved spectra for various delay times after excitation at 400 nm. The heating induced absorption change (black line, cf. d) is added to demonstrate that the system progresses toward its intramolecular equilibrium for longer delay times. The green arrow marks the shoulder developing with internal energy conversion. (b) Temporal evolution at the spectral positions marked by arrows in (a). Solid lines show a multiexponential fit. Dynamics are dominated by the vibration-vibrational relaxation time τ_{vib} = (37 ± 4) ps and the lifetime of the singlet excited state $\tau_{S1} \approx 3$ ns. (c) FTIR absorbance changes for various temperature differences in steps of 10 K. (d) Normalized spectra from (c) reveal that the spectral shape is independent of temperature. Data are corrected by solvent background.

vibrational or the metal phonon bath-vibrational relaxation rates are known. The vibrational modes are allowed to relax anharmonically to higher or lower energy modes ν_{q+n} or ν_{q-n} with a rate γ_{vib} and to the metal phonon bath with a rate γ_{ph} (Figure 3c). IR time-resolved spectroscopy on **BPA** in solution provides direct information on the internal equilibration time[53] (τ_{vib}) (see Methods and Supporting Information Figures, cf. Figures S8−S12). The time-dependent spectral dynamics of **BPA** dissolved in dichloromethane, shown in Figure 4a,b, yield an internal vibrational-vibrational relaxation time τ_{vib} = (37 ± 4) ps. Note that, in experiments on larger molecules attached to a surface in dry surroundings, no significant change of the internal vibrational relaxation dynamics has been observed, compared to the same molecule in solution.[54,55] The determined internal relaxation time τ_{vib} is in line with reduced vibration-vibrational coupling constants in anthracene derivatives substituted at the 9,10 position, as in **BPA**.[56] The time scale agrees with common estimates, placing intramolecular relaxation redistribution times between 10 and 100 ps.[57]

To account for different coupling strengths per mode, we calculate the theoretical EPC strengths for the normal modes (ν_q) via DFT[58,59] according to the molecular-junction configuration presented in Figure 3a. In the rate equation model for the steady state vibrational distribution,

$$\frac{dp_q}{dt} = \frac{I}{e}\cdot\lambda_q - \gamma_{vib}\cdot p_q + \gamma_{vib}\cdot p_{q\pm1} - \gamma_{ph}\cdot p_q \qquad (2)$$

the coupling strength of an individual mode $\lambda_q = w_q\lambda$ is determined by the relative contribution w_q to the total EPC constant λ. The calculated scaling factors w_q are shown in the table in Figure 3b, and we assume that their distribution remains valid under the steady-state conditions of the experiment. Figure 3b indicates that only the lowest energy modes contribute significantly to the EPC. Analogously, low-energy modes have been shown to be of primary relevance for EPC during charge transport in benzene,[14,60] fullerene,[27,31] and carbon nanotubes.[21,61] Similarly, the collective excitation of closely spaced modes at low biases strongly contributes to the prominent inelastic tunneling spectroscopy signal of oligo-(phenyl-ethynylene) junctions.[62] With these considerations, the N steady-state linear equations are solved self-consistently, one for the population of each of **BPA**'s vibrational modes (each mode's energy calculated from DFT). Solving the steady-state rate equations with a current of 35 nA and an internal relaxation time of τ_{vib} = (37 ± 4) ps yields the best fit to the experimental data with a total EPC constant of λ = 0.48 and an R-factor of 0.001 (Figure 3b,d). The envelope for the vibrational population derived from the model is shown with a red line in Figure 3d, together with the measured vibrational population (blue line).

To further substantiate our model and theory, we employ an independent solid-state model. According to the nonequilibrium model[20] the strength of the EPC given by the second moment of the Eliashberg spectral function is:

$$\lambda\langle\nu^2\rangle = \frac{k_B T_l}{3c^2 h\tau_{vib}} \qquad (3)$$

Here $\langle\nu^2\rangle$ is the square of the characteristic vibrational frequency (in wavenumbers), and T_l is the inner-molecular lattice temperature. The latter is expected to be close to the solvent temperature; that is, $T_l \approx 300$ K.[20] Upon posing a coupling constant of λ = 0.48 this model yields a characteristic vibrational frequency of ∼11.4 cm^{-1}. This small characteristic frequency provides further evidence that the low-energy vibrational modes govern the EPC in the studied junction.

CONCLUSIONS

By measuring the steady-state distribution of the vibrational population on current-carrying molecules with Raman spectroscopy we determine the electron−phonon coupling strength of charges passing through the molecular junction and the dissipation of phonons to the electrodes. Complementary time-resolved IR spectroscopy and theory provide the time constant for internal redistribution of vibrations and the

https://dx.doi.org/10.1021/jacs.9b07757
J. Am. Chem. Soc. 2020, 142, 3384−3391

distribution of the coupling strengths to the individual modes. By generalizing the use of the MJS approach, we expect that the identification and quantification of vibrational modes involved in phenomena like charge transport, heat dissipation, or energy loss mechanisms, will become accessible. Such studies are decisive for the determination of electron−phonon coupling and inference effects in specific molecular quantum vibronic states, which is a prerequisite for the advancement of molecular-scale electronics and related fields.

■ ASSOCIATED CONTENT

Supporting Information

The Supporting Information is available free of charge at https://pubs.acs.org/doi/10.1021/jacs.9b07757.

Additional details on experimental procedures, and detailed description of the rate model, schematics, statistical correlations of simulated Raman spectra to experiment, Raman spectrum at 100 °C and below the cutoff frequency at 600 cm^{-1}, computed charge-vibrational coupling to different low-lying modes. Steady-state and transient spectroscopy on **BPA** in dichloromethane and additional references (PDF).

■ AUTHOR INFORMATION

Corresponding Authors

Carlos-Andres Palma − *Physics Department, Technical University of Munich, 85748 Garching, Germany; Institute of Physics, Chinese Academy of Sciences, 100190 Beijing, P. R. China; Department of Physics & IRIS Adlershof, Humboldt-Universität zu Berlin, 12489 Berlin, Germany;* orcid.org/0000-0001-5576-8496; Email: palma@iphy.ac.cn

Hristo Iglev − *Physics Department, Technical University of Munich, 85748 Garching, Germany*; Email: hristo.iglev@tum.de

Johannes V. Barth − *Physics Department, Technical University of Munich, 85748 Garching, Germany;* orcid.org/0000-0002-6270-2150; Email: jvb@tum.de

Joachim Reichert − *Physics Department, Technical University of Munich, 85748 Garching, Germany;* orcid.org/0000-0002-8843-3972; Email: joachim.reichert@tum.de

Authors

Hai Bi − *Physics Department, Technical University of Munich, 85748 Garching, Germany*

Yuxiang Gong − *Physics Department, Technical University of Munich, 85748 Garching, Germany*

Klara Stallhofer − *Physics Department, Technical University of Munich, 85748 Garching, Germany;* orcid.org/0000-0001-6314-0156

Matthias Nuber − *Physics Department, Technical University of Munich, 85748 Garching, Germany;* orcid.org/0000-0002-4409-3590

Chao Jing − *Physics Department, Technical University of Munich, 85748 Garching, Germany*

Felix Meggendorfer − *Physics Department, Technical University of Munich, 85748 Garching, Germany*

Shizheng Wen − *Beijing Computational Science Research Center, 100084 Beijing, P. R. China;* orcid.org/0000-0002-0316-1323

ChiYung Yam − *Beijing Computational Science Research Center, 100084 Beijing, P. R. China;* orcid.org/0000-0002-3860-2934

Reinhard Kienberger − *Physics Department, Technical University of Munich, 85748 Garching, Germany*

Mark Elbing − *Department of Applied Natural Sciences, TH Lübeck, 23562 Lübeck, Germany*

Marcel Mayor − *Institute of Nanotechnology, Karlsruhe Institute of Technology, 76344 Karlsruhe, Germany; Department of Chemistry, University of Basel, CH-4056 Basel, Switzerland;* orcid.org/0000-0002-8094-7813

Complete contact information is available at: https://pubs.acs.org/10.1021/jacs.9b07757

Author Contributions

○Equally contributing authors.

Notes

The authors declare no competing financial interest.

■ ACKNOWLEDGMENTS

We acknowledge the Deutsche Forschungsgemeinschaft for financial support via the SPP 1234 (Grant No. RE2592), Germany's Excellence Strategy (Munich Centre for Advanced Photonics and e-conversion Cluster of Excellence EXC 2089/1-390776260), the European Research Council via Advanced Grant MolArt (Grant No. 247299), the China Scholarship Council, the European Union's Horizon 2020 research and innovation programme under Grant 664878, the National Natural Science Foundation of China (21673017 and U1530401), and the Alexander von Humboldt Foundation. We thank A. Holleitner at the Zentrum für Nanotechnologie und Nanomaterialien, together with R. Bader and M. Bopp at the Leibniz-Rechenzentrum for infrastructure support, and A. C. Papageorgiou, W. Zhou, L. C. Lacroix as well as E. Scheer for discussions. We warmly acknowledge femtosecond IR spectroscopy infrastructure support and discussions by W. Zinth.

■ REFERENCES

(1) Galperin, M.; Ratner, M. A.; Nitzan, A.; Troisi, A. Nuclear coupling and polarization in molecular transport junctions: Beyond tunneling to function. *Science* **2008**, *319* (5866), 1056−1060.

(2) Palma, C.-A.; Samorí, P. Blueprinting macromolecular electronics. *Nat. Chem.* **2011**, *3* (6), 431−436.

(3) Shulaker, M. M.; Hills, G.; Patil, N.; Wei, H.; Chen, H. Y.; Wong, H. S. P.; Mitra, S. Carbon nanotube computer. *Nature* **2013**, *501* (7468), 526−529.

(4) Reed, M. A.; Zhou, C.; Muller, C. J.; Burgin, T. P.; Tour, J. M. Conductance of a molecular junction. *Science* **1997**, *278* (5336), 252−254.

(5) Frank, S.; Poncharal, P.; Wang, Z. L.; de Heer, W. A. Carbon nanotube quantum resistors. *Science* **1998**, *280* (5370), 1744−1746.

(6) Lang, N. D.; Avouris, P. Electrical conductance of individual molecules. *Phys. Rev. B: Condens. Matter Mater. Phys.* **2001**, *64* (12), 125323.

(7) Smit, R. H. M.; Noat, Y.; Untiedt, C.; Lang, N. D.; van Hemert, M. C.; van Ruitenbeek, J. M. Measurement of the conductance of a hydrogen molecule. *Nature* **2002**, *419* (6910), 906−909.

(8) Reichert, J.; Ochs, R.; Beckmann, D.; Weber, H. B.; Mayor, M.; von Lohneysen, H. Driving current through single organic molecules. *Phys. Rev. Lett.* **2002**, *88* (17), 176804.

(9) Lindsay, S. M.; Ratner, M. A. Molecular transport junctions: Clearing mists. *Adv. Mater.* **2007**, *19* (1), 23−31.

(10) Yelin, T.; Korytar, R.; Sukenik, N.; Vardimon, R.; Kumar, B.; Nuckolls, C.; Evers, F.; Tal, O. Conductance saturation in a series of highly transmitting molecular junctions. *Nat. Mater.* **2016**, *15* (4), 444−449.

(11) Xiang, D.; Wang, X.; Jia, C.; Lee, T.; Guo, X. Molecular-Scale Electronics: From Concept to Function. *Chem. Rev.* **2016**, *116* (7), 4318−4440.
(12) Giustino, F. Electron-phonon interactions from first principles. *Rev. Mod. Phys.* **2017**, *89* (1), 015003.
(13) Cuevas, J. C.; Scheer, E. *Molecular Electronics: An Introduction to Theory and Experiment,* 1st ed.; World Scientific Publishing Company: Singapore, 2010.
(14) Sergueev, N.; Roubtsov, D.; Guo, H. Ab initio analysis of electron-phonon coupling in molecular devices. *Phys. Rev. Lett.* **2005**, *95* (14), 146803.
(15) Tao, N. J. Electron transport in molecular junctions. *Nat. Nanotechnol.* **2006**, *1* (3), 173−181.
(16) Pop, E. Energy Dissipation and Transport in Nanoscale Devices. *Nano Res.* **2010**, *3* (3), 147−169.
(17) Ballmann, S.; Hartle, R.; Coto, P. B.; Elbing, M.; Mayor, M.; Bryce, M. R.; Thoss, M.; Weber, H. B. Experimental Evidence for Quantum Interference and Vibrationally Induced Decoherence in Single-Molecule Junctions. *Phys. Rev. Lett.* **2012**, *109* (5), 056801.
(18) Hartle, R.; Butzin, M.; Thoss, M. Vibrationally induced decoherence in single-molecule junctions. *Phys. Rev. B: Condens. Matter Mater. Phys.* **2013**, *87* (8), 085422.
(19) Chang, C. T. C.; Sethna, J. P.; Pasupathy, A. N.; Park, J.; Ralph, D. C.; McEuen, P. L. Phonons and conduction in molecular quantum dots: Density functional calculations of Franck-Condon emission rates for bifullerenes in external fields. *Phys. Rev. B: Condens. Matter Mater. Phys.* **2007**, *76* (4), 045435.
(20) Gadermaier, C.; Alexandrov, A. S.; Kabanov, V. V.; Kusar, P.; Mertelj, T.; Yao, X.; Manzoni, C.; Brida, D.; Cerullo, G.; Mihailovic, D. Electron-Phonon Coupling in High-Temperature Cuprate Superconductors Determined from Electron Relaxation Rates. *Phys. Rev. Lett.* **2010**, *105*, 257001.
(21) Leturcq, R.; Stampfer, C.; Inderbitzin, K.; Durrer, L.; Hierold, C.; Mariani, E.; Schultz, M. G.; von Oppen, F.; Ensslin, K. Franck-Condon blockade in suspended carbon nanotube quantum dots. *Nat. Phys.* **2009**, *5* (5), 327−331.
(22) van der Lit, J.; Boneschanscher, M. P.; Vanmaekelbergh, D.; Ijas, M.; Uppstu, A.; Ervasti, M.; Harju, A.; Liljeroth, P.; Swart, I. Suppression of electron-vibron coupling in graphene nanoribbons contacted via a single atom. *Nat. Commun.* **2013**, *4*, 2023.
(23) Stipe, B. C.; Rezaei, M. A.; Ho, W. Single-molecule vibrational spectroscopy and microscopy. *Science* **1998**, *280* (5370), 1732−1735.
(24) Nazin, G. V.; Wu, S. W.; Ho, W. Tunneling rates in electron transport through double-barrier molecular junctions in a scanning tunneling microscope. *Proc. Natl. Acad. Sci. U. S. A.* **2005**, *102* (25), 8832−8837.
(25) Pavliček, N.; Swart, I.; Niedenführ, J.; Meyer, G.; Repp, J. Symmetry Dependence of Vibration-Assisted Tunneling. *Phys. Rev. Lett.* **2013**, *110* (13), 136101.
(26) Schinabeck, C.; Erpenbeck, A.; Hartle, R.; Thoss, M. Hierarchical quantum master equation approach to electronic-vibrational coupling innonequilibrium transport through nanosystems. *Phys. Rev. B: Condens. Matter Mater. Phys.* **2016**, *94*, 201407.
(27) Park, H.; Park, J.; Lim, A. K. L.; Anderson, E. H.; Alivisatos, A. P.; McEuen, P. L. Nanomechanical oscillations in a single-C-60 transistor. *Nature* **2000**, *407* (6800), 57−60.
(28) Osorio, E. A.; O'Neill, K.; Stuhr-Hansen, N.; Nielsen, O. F.; Bjornholm, T.; van der Zant, H. S. J. Addition energies and vibrational fine structure measured in electromigrated single-molecule junctions based on an oligophenylenevinylene derivative. *Adv. Mater.* **2007**, *19* (2), 281−285.
(29) Hihath, J.; Arroyo, C. R.; Rubio-Bollinger, G.; Tao, N. J.; Agraït, N. Study of electron-phonon interactions in a single molecule covalently connected to two electrodes. *Nano Lett.* **2008**, *8* (6), 1673−1678.
(30) Buttiker, M.; Imry, Y.; Landauer, R.; Pinhas, S. Generalized Many-Channel Conductance Formula with Application to Small Rings. *Phys. Rev. B: Condens. Matter Mater. Phys.* **1985**, *31* (10), 6207−6215.
(31) Braig, S.; Flensberg, K. Vibrational sidebands and dissipative tunneling in molecular transistors. *Phys. Rev. B: Condens. Matter Mater. Phys.* **2003**, *68* (20), 205324.
(32) Seldenthuis, J. S.; van der Zant, H. S. J.; Ratner, M. A.; Thijssen, J. M. Vibrational excitations in weakly coupled single-molecule junctions: A computational analysis. *ACS Nano* **2008**, *2* (7), 1445−1451.
(33) Bi, H.; Palma, C.-A.; Gong, Y.; Hasch, P.; Elbing, M.; Mayor, M.; Reichert, J.; Barth, J. V. Voltage-Driven Conformational Switching with Distinct Raman Signature in a Single-Molecule Junction. *J. Am. Chem. Soc.* **2018**, *140* (14), 4835−4840.
(34) Li, Y.; Doak, P.; Kronik, L.; Neaton, J. B.; Natelson, D. Voltage tuning of vibrational mode energies in single-molecule junctions. *Proc. Natl. Acad. Sci. U. S. A.* **2014**, *111* (4), 1282−1287.
(35) Li, Y. J.; Zolotavin, P.; Doak, P.; Kronik, L.; Neaton, J. B.; Natelson, D. Interplay of Bias-Driven Charging and the Vibrational Stark Effect in Molecular Junctions. *Nano Lett.* **2016**, *16* (2), 1104−1109.
(36) Liu, Z.; Ding, S. Y.; Chen, Z. B.; Wang, X.; Tian, J. H.; Anema, J. R.; Zhou, X. S.; Wu, D. Y.; Mao, B. W.; Xu, X.; Ren, B.; Tian, Z. Q. Revealing the molecular structure of single-molecule junctions in different conductance states by fishing-mode tip-enhanced Raman spectroscopy. *Nat. Commun.* **2011**, *2*, 305.
(37) Aradhya, S. V.; Venkataraman, L. Single-molecule junctions beyond electronic transport. *Nat. Nanotechnol.* **2013**, *8* (6), 399−410.
(38) Mitra, A.; Aleiner, I.; Millis, A. J. Phonon effects in molecular transistors: Quantal and classical treatment. *Phys. Rev. B: Condens. Matter Mater. Phys.* **2004**, *69* (24), 245302.
(39) Koch, J.; Semmelhack, M.; von Oppen, F.; Nitzan, A. Current-induced nonequilibrium vibrations in single-molecule devices. *Phys. Rev. B: Condens. Matter Mater. Phys.* **2006**, *73* (15), 155306.
(40) Fischer, U. C.; Koglin, J.; Fuchs, H. The Tetrahedral Tip as a Probe for Scanning near-Field Optical Microscopy at 30-Nm Resolution. *J. Microsc. (Oxford, U. K.)* **1994**, *176*, 231−237.
(41) Koglin, J.; Fischer, U. C.; Fuchs, H. Material contrast in scanning near-field optical microscopy at 1−10 nm resolution. *Phys. Rev. B: Condens. Matter Mater. Phys.* **1997**, *55* (12), 7977−7984.
(42) Domke, K. F.; Zhang, D.; Pettinger, B. Enhanced Raman spectroscopy: Single molecules or carbon? *J. Phys. Chem. C* **2007**, *111* (24), 8611−8616.
(43) Benz, F.; Schmidt, M. K.; Dreismann, A.; Chikkaraddy, R.; Zhang, Y.; Demetriadou, A.; Carnegie, C.; Ohadi, H.; de Nijs, B.; Esteban, R.; Aizpurua, J.; Baumberg, J. J. Single-molecule optomechanics in "picocavities". *Science* **2016**, *354* (6313), 726−729.
(44) Venkataraman, L.; Klare, J. E.; Nuckolls, C.; Hybertsen, M. S.; Steigerwald, M. L. Dependence of single-molecule junction conductance on molecular conformation. *Nature* **2006**, *442* (7105), 904−907.
(45) Galperin, M.; Ratner, M. A.; Nitzan, A. Inelastic electron tunneling spectroscopy in molecular junctions: Peaks and dips. *J. Chem. Phys.* **2004**, *121* (23), 11965−11979.
(46) Otto, A.; Futamata, M. Electronic mechanisms of SERS. *Top Appl. Phys.* **2006**, *103*, 147−182.
(47) Ioffe, Z.; Shamai, T.; Ophir, A.; Noy, G.; Yutsis, I.; Kfir, K.; Cheshnovsky, O.; Selzer, Y. Detection of heating in current-carrying molecular junctions by Raman scattering. *Nat. Nanotechnol.* **2008**, *3* (12), 727−732.
(48) Ward, D. R.; Corley, D. A.; Tour, J. M.; Natelson, D. Vibrational and electronic heating in nanoscale junctions. *Nat. Nanotechnol.* **2011**, *6* (1), 33−38.
(49) Galperin, M.; Nitzan, A. Raman scattering from biased molecular conduction junctions: The electronic background and its temperature. *Phys. Rev. B: Condens. Matter Mater. Phys.* **2011**, *84* (19), 195325.
(50) Lee, W.; Kim, K.; Jeong, W.; Zotti, L. A.; Pauly, F.; Cuevas, J. C.; Reddy, P. Heat dissipation in atomic-scale junctions. *Nature* **2013**, *498* (7453), 209−212.

https://dx.doi.org/10.1021/jacs.9b07757
J. Am. Chem. Soc. 2020, 142, 3384−3391

(51) Agraït, N.; Untiedt, C.; Rubio-Bollinger, G.; Vieira, S. Onset of energy dissipation in ballistic atomic wires. *Phys. Rev. Lett.* **2002**, *88* (21), 216803.
(52) Gao, M.; Li, Q.-Z.; Yan, X.-W.; Wang, J. Prediction of phonon-mediated superconductivity in borophene. *Phys. Rev. B: Condens. Matter Mater. Phys.* **2017**, *95* (2), 024505.
(53) Iglev, H.; Schmeisser, M.; Simeonidis, K.; Thaller, A.; Laubereau, A. Ultrafast superheating and melting of ice. *Nature* **2006**, *439*, 183−186.
(54) Ricks, A. M.; Anfuso, C. L.; Rodríguez-Córdoba, W.; Lian, T. Vibrational relaxation dynamics of catalysts on TiO2 Rutile (110) single crystal surfaces and anatase nanoporous thin films. *Chem. Phys.* **2013**, *422*, 264−271.
(55) Anfuso, C. L.; Ricks, A. M.; Rodríguez-Cordoba, W.; Lian, T. Ultrafast vibrational relaxation dynamics of a rhenium bipyridyl CO2−reduction catalyst at a Au electrode surface probed by time-resolved vibrational sum frequency generation spectroscopy. *J. Phys. Chem. C* **2012**, *116* (50), 26377−26384.
(56) Uejima, M.; Sato, T.; Tanaka, K.; Kaji, H. Enhancement of fluorescence in anthracene by chlorination: Vibronic coupling and transition dipole moment density analysis. *Chem. Phys.* **2014**, *430*, 47−55.
(57) Yoo, H. S.; DeWitt, M. J.; Pate, B. H. Vibrational dynamics of terminal acetylenes: I. Comparison of the intramolecular vibrational energy redistribution rate of gases and the total relaxation rate of dilute solutions at room temperature. *J. Phys. Chem. A* **2004**, *108* (8), 1348−1364.
(58) Frederiksen, T.; Paulsson, M.; Brandbyge, M.; Jauho, A.-P. Inelastic transport theory from first principles: Methodology and application to nanoscale devices. *Phys. Rev. B: Condens. Matter Mater. Phys.* **2007**, *75* (20), 205413.
(59) Mazzola, F.; Frederiksen, T.; Balasubramanian, T.; Hofmann, P.; Hellsing, B.; Wells, J. W. Strong electron-phonon coupling in the σ band of graphene. *Phys. Rev. B: Condens. Matter Mater. Phys.* **2017**, *95* (7), 075430.
(60) Karimi, M. A.; Bahoosh, S. G.; Herz, M.; Hayakawa, R.; Pauly, F.; Scheer, E. Shot Noise of 1,4-Benzenedithiol Single-Molecule Junctions. *Nano Lett.* **2016**, *16* (3), 1803−1807.
(61) LeRoy, B. J.; Lemay, S. G.; Kong, J.; Dekker, C. Electrical generation and absorption of phonons in carbon nanotubes. *Nature* **2004**, *432* (7015), 371−374.
(62) Long, D. P.; Lazorcik, J. L.; Mantooth, B. A.; Moore, M. H.; Ratner, M. A.; Troisi, A.; Yao, Y.; Ciszek, J. W.; Tour, J. M.; Shashidhar, R. Effects of hydration on molecular junction transport. *Nat. Mater.* **2006**, *5* (11), 901−908.

https://dx.doi.org/10.1021/jacs.9b07757
J. Am. Chem. Soc. 2020, 142, 3384−3391